Optical conductivity of granular aluminum films near the Mott metal-to-insulator transition

Aviv Glezer Moshe,[1,2,*] Eli Farber,[2] and Guy Deutscher[1]
[1]*Raymond and Beverly Sackler School of Physics and Astronomy, Tel Aviv University, Tel Aviv 6997801, Israel*
[2]*Department of Physics and Department of Electrical and Electronic Engineering, Ariel University, Ariel*

(Received 7 January 2019; revised manuscript received 15 May 2019; published 5 June 2019)

We report measurements of the energy gap of granular aluminum films by THz spectroscopy. We find that as the grains progressively decouple, the coupling ratio $2\Delta(0)/k_BT_c$ increases above the BCS weak-coupling ratio 3.53, and reaches values consistent with an approach to BCS-BEC crossover for the high-resistivity samples, expected from the short coherence length. The Mattis-Bardeen theory describes remarkably well the behavior of $\sigma_{1,s}/\sigma_{1,n}$ for all samples up to very high normal-state resistivities.

DOI: 10.1103/PhysRevB.99.224503

I. INTRODUCTION

In granular superconductors, electrons are confined inside nanoscale metallic grains due to intergrain oxide barriers, which reduces the value of the coherence length. When the barrier thickness is increased, the coherence volume can decrease up to a point where the number of Cooper pairs that it contains is of the order of unity. Thereby, a crossover from a BCS regime, where the number of pairs per coherence volume is very large, to a BEC condensation, where it is of the order of unity, is expected. However, a detailed comparison with experiments has been difficult because of a lack of theoretical studies of the BCS-to-BEC crossover regime. But, recently, detailed theoretical predictions regarding the evolution of the strong-coupling ratio around this crossover have become available [1,2]. We show here that they are in quantitative agreement with our experimental findings, obtained on granular aluminum films from THz optical conductivity measurements in the vicinity of the metal-to-insulator transition.

We find that up to that transition, the optical gap edge remains well defined, and that contrary to the behavior of disordered NbN films [3], the ratio $2\Delta(0)/k_BT_c$ increases with resistivity, reaching a value of 4.51 in the highest-resistivity sample ($\sim$8000 $\mu\Omega$ cm) studied.

According to the recent work of Pisani *et al.* [1,2], the strong-coupling ratio increases when the BCS-to-BEC crossover is approached. The highest-resistivity sample that we have studied falls in the range where the strong-coupling ratio is substantially enhanced. It is consistent with the experimental value of the coherence length.

In view of their possible applications as high kinetic inductance elements in quantum circuits (QCs), there has recently been renewed interest in the properties of strongly disordered superconductors in the vicinity of the metal-to-insulator (M-I) transition. The optical properties of disordered NbN films have been the focus of particular attention [3,4]. It was found that in these films, where disorder has a homogeneous distribution on the atomic scale, the coupling ratio $2\Delta(0)/k_BT_c$ decreases continuously below the weak-coupling limit value 3.53 when disorder is increased. This decrease becomes very pronounced when the parameter k_Fl, where k_F is the Fermi wave vector and l is the electron mean free path, becomes of the order of unity [3]. At the highest resistivity investigated ($\sim$1000 $\mu\Omega$ cm), there is not even a clear optical gap edge. At the same time, the coupling ratio obtained from the tunneling gap remains at about 4.2. This behavior departs from the predictions of the BCS Mattis-Bardeen theory [5]. The enhanced low-frequency dissipation has detrimental consequences on the quality factor of high-impedance resonators that could be used in QCs [6].

The behavior of granular Al is more favorable for QC applications. We propose that the difference in behavior between NbN and granular Al films stems from the different nature of the metal-to-insulator transition, being of the Anderson type in the former [7] and of the Mott type in the latter [8].

II. EXPERIMENT AND METHODS

Granular aluminum thin films were prepared by thermal evaporation of clean Al pallets in a controlled O_2 pressure, where the base pressure of the vacuum chamber is $\sim 1\times10^{-7}$ Torr. The films were deposited onto liquid-nitrogen-cooled substrates [$10\times10\times2$ mm^3 MgO or $10\times10\times1$ mm^3 $(LaAlO_3)_{0.3}$-$(SrAl_{0.5}Ta_{0.5}O_3)_{0.7}$ (LSAT), which result in a similar Fabry-Perot pattern in the optical spectra]. Films with various degree of grain coupling were obtained by varying the O_2 partial pressure in the range of 2–5 $\times10^{-5}$ Torr, while keeping the deposition rate about 5 ± 1 A/s, similar to previous work [9,10]. The films' thickness varied in the range 40–100 nm in order to obtain high-quality transmission measurements as the resistivity of the films increases.

Standard four-point resistivity measurements were performed in either a commercial QD PPMS or in a home-built probe; we characterize each film by its normal-state resistivity ρ_n at 4.2 K. Great care was taken to obtain homogeneous films. Sharp superconducting transitions were obtained even for the highest-resistivity films; see Fig. 3.

The optical spectroscopy measurements were done by utilizing a quasioptical Mach-Zehnder interferometer, which

*avivmoshe@mail.tau.ac.il

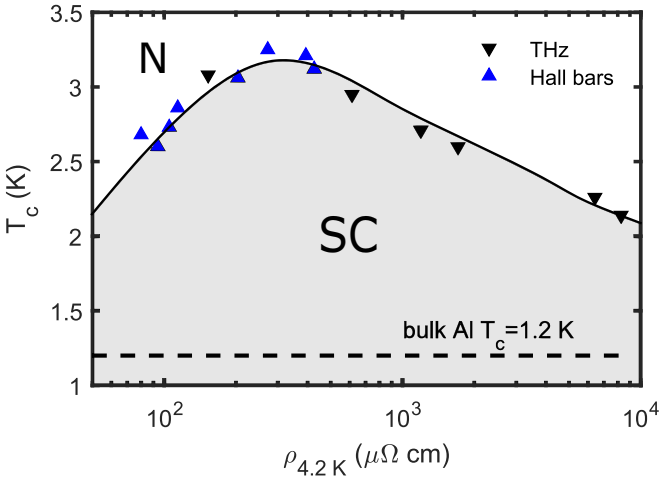

FIG. 1. Critical temperature of studied granular aluminum films vs the normal-state resistivity. Black upside-down triangles (▼) marks T_c of the optical spectroscopy studied samples. Blue triangles (▲) marks T_c as measured by Hall bars with similar deposition conditions as described in the main text. The dashed line marks the bulk aluminum critical temperature.

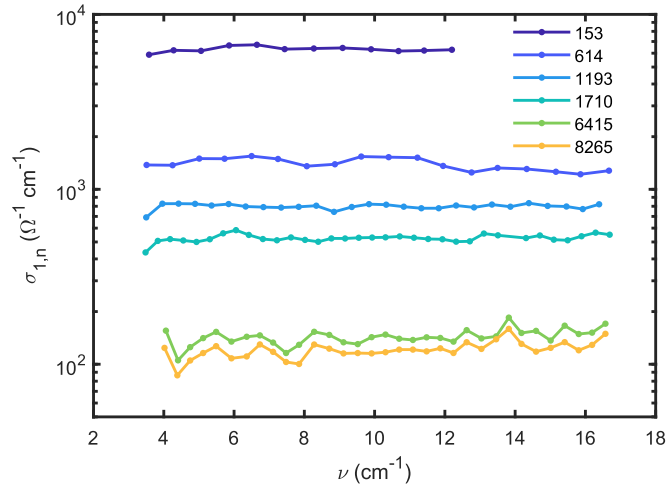

FIG. 2. Real part of the optical conductivity at 4.2 K for all samples. The legend marks the normal-state resistivity in $\mu\Omega$ cm as obtained from transport measurements of the same samples.

allows us to obtain the complex transmission $\hat{t} = |t|e^{i\phi_t}$ [9,11] of the substrate-film system. The radiation sources are tunable monochromatic backward-wave oscillators (BWO); by utilizing several sources, we cover a frequency range of 3–17 cm^{-1} (or about 0.1–0.5 THz). A commercial optical ^{4}He cryostat with a home-built sample holder provides us with a dynamic temperature range down to 1.5 K and the ability to measure up to two samples during one cooldown. The complex transmission was measured for all samples at 4.2 K and at various temperatures close to and below T_c, down to 1.5 K. Then the complex conductivity $\hat{\sigma}(\omega) = \sigma_1(\omega) + i\sigma_2(\omega)$ is calculated from the measured complex transmission via the Fresnel equations [11,12], without relying on any microscopic model.

III. RESULTS

Figure 1 shows the superconducting (SC) critical temperature as a function of the normal-state resistivity at 4.2 K for films studied in this work and also that of Hall bars prepared separately in our laboratory. The well-known "dome"-shaped phase diagram [9,13–15] can be clearly seen.

To allow an easy comparison with the behavior of NbN films [3,4], our main results are displayed in Table I. To evaluate $k_F l$, we approximate it by the free-electron formula $k_F l = \frac{m}{\hbar}\frac{1}{\rho} v_F \rho l$ by using the values of $v_F = 15.99 \times 10^7$ cm/s and $\rho l = 5.01 \times 10^{-6}$ $\mu\Omega$ cm^2 as obtained by Gall [16] for clean aluminum. For all samples, except for sample 1, the value of $k_F l$ is equal to or smaller than one, in sharp contrast with the behavior of the studied NbN films [3,4].

TABLE I. Properties of the studied samples.

Sample ID	ρ_{300K} ($\mu\Omega$ cm)	$\rho^n_{4.2K}$ ($\mu\Omega$ cm)	$k_F l$	T_c (K)	$\frac{2\Delta(0)}{k_B T_c}$
1	155	153	4.38	3.08	3.56
2	589	614	1.00	2.95	3.64
3	1047	1193	0.55	2.71	3.73
4	1482	1710	0.36	2.60	3.77
5	5131	6415	0.10	2.26	4.29
6	6344	8265	0.085	2.14	4.51

The normal-state conductivity $\sigma_{1,n}$ as measured at 4.2 K is frequency independent up to 17 cm^{-1}; see Fig. 2. The resistive SC transition for all studied samples, along with their measured SC gap $\Delta(T)$ as a function of reduced temperature T/T_c, is presented in Fig. 3, where we define T_c as the temperature where the resistivity has decreased below 1% of its normal-state value. Up to the highest-resistivity samples, the superconducting transition is well defined; see Fig. 4.

In the superconducting state, a good fit to the Mattis-Bardeen (MB) theory [5] is obtained for all samples up to resistivities of about 8000 $\mu\Omega$ cm, as one can see in Fig. 5. The values of $\Delta(0)$ used in Table I were obtained from these fits.

In Figs. 2, 5, and 6, the frequency ν is given in units of cm^{-1}, which is related to ω by $\omega = 2\pi c\nu$, where c is the speed of light in cm/sec. We analyze the optical data similarly to the method used by Pracht *et al.* [9]. Representative transmission $|t|^2$ and frequency-normalized phase spectra ϕ/ν are shown in Fig. 6, for both the normal (at 4.2 K) and superconducting states. The strong oscillation pattern is due to multiple reflections inside the substrate. Utilizing the Fresnel equations for multiple reflections in a bilayer system [11,12,17], we obtain the complex conductivity $\hat{\sigma}(\omega) = \sigma_1(\omega) + i\sigma_2(\omega)$, without relying on any microscopic model. The measured transmission depends on both the substrate and film dielectric function $\hat{\epsilon}(\omega)$ and thickness

$$\hat{t} = t\left[d_s, \epsilon_1^s(\omega), \epsilon_2^s(\omega); d_f, \epsilon_1^f(\omega), \epsilon_2^f(\omega)\right], \tag{1}$$

where $\hat{\epsilon}(\omega) = \epsilon_1(\omega) + i\epsilon_2(\omega)$, which can be expressed as complex conductivity $\hat{\sigma}(\omega)$ by the relation

$$\hat{\epsilon}(\omega) = 1 + i\frac{2\pi}{\epsilon_0}\frac{\hat{\sigma}(\omega)}{\omega}. \tag{2}$$

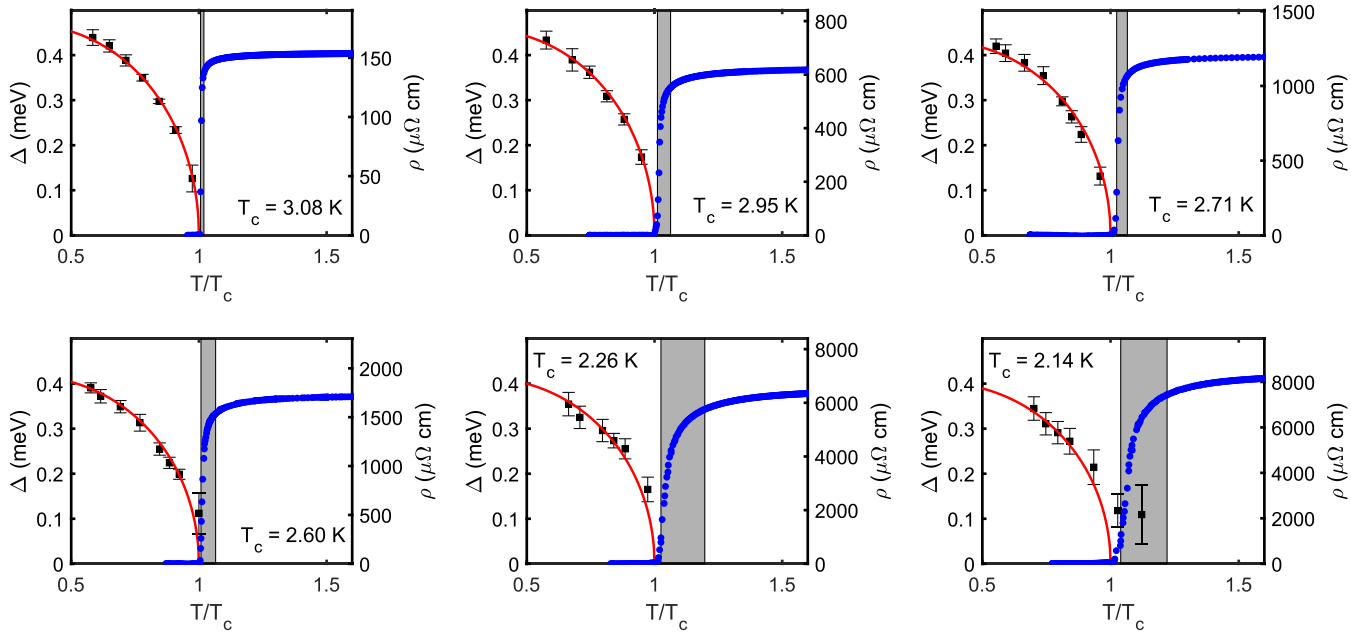

FIG. 3. $\Delta(T)$ and $\rho(T)$ vs temperature for all studied samples. Black squares (■) are the measured gap, obtained by fitting $\sigma_{1,s}/\sigma_{1,n}$ to MB formulas, and the red curve is a fit to a BCS gap equation curve. Blue circles (•) are the measured resistivity and the gray area marks the decrease of the normal-state resistivity from 90 to 10% of its normal-state value.

Once $\hat{t}$ is measured, we need to disentangle the substrate contribution in order to extract the complex conductivity of the film. The MgO and LSAT dielectric substrates are known to be completely transparent (means $\epsilon_2^s = 0$) in the THz frequency range [9,18], as we also checked in a separate experiment. We first analyze the normal state at 4.2 K, where the normal-state conductivity obeys the Drude model with high scattering rate relative to the measured frequency range, in this low-frequency regime $\sigma_2 \simeq 0$. We fit around each maxima/minima in the spectra with σ_1 of the film and ϵ_1 of the substrate. We then use the obtained set of ϵ_1 for the low-temperature data, where we fit around each maxima/minima by both σ_1, σ_2 of the film. This process yields a pair of σ_1, σ_2 for each frequency point, as can be shown in Fig. 6.

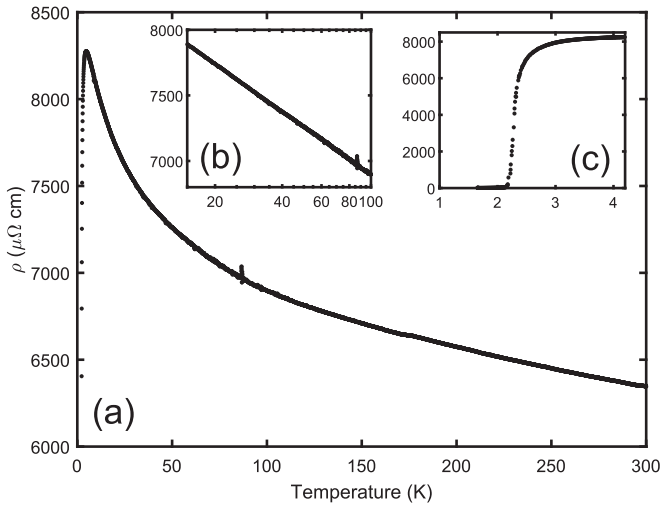

FIG. 4. (a) Resistivity as a function of temperature of sample 6. Insets (b) and (c) are the same data focused on different temperatures scales: (b) The temperature is presented in a logarithmic scale, which shows a logarithmic increase of ρ over wide range of temperatures; (c) the resistive SC transition.

Once we obtain $\hat{\sigma}(\omega, T)$, we fit it to the Mattis-Bardeen (MB) formulas [5], which are appropriate since we are well within the dirty limit $\Delta \ll \hbar/\tau$ [9,10,19],

$$\frac{\sigma_1(\omega)}{\sigma_n} = \frac{e^2 n_s}{m^* \sigma_n}\pi\delta(\omega) + \frac{2}{\hbar\omega}\int_{\Delta}^{\infty} dE\, g(E)[f(E) - f(E+\hbar\omega)] - \frac{\Theta(\hbar\omega - 2\Delta)}{\hbar\omega}\int_{\Delta-\hbar\omega}^{-\Delta} dE\, g(E)[1 - 2f(E+\hbar\omega)], \tag{3}$$

$$\frac{\sigma_2(\omega)}{\sigma_n} = \frac{1}{\hbar\omega}\int_{\max\{-\Delta,\Delta-\hbar\omega\}}^{\Delta} dE\, g(E)[1 - 2f(E+\hbar\omega)] \times \frac{E(E+\hbar\omega) + \Delta^2}{\sqrt{\Delta^2 - E^2}\sqrt{(E+\hbar\omega)^2 - \Delta^2}}, \tag{4}$$

$$g(E) = \frac{E(E+\hbar\omega) + \Delta^2}{\sqrt{E^2 - \Delta^2}\sqrt{(E+\hbar\omega)^2 - \Delta^2}}. \tag{5}$$

The normal-state conductivity is determined as $\sigma_1(\omega)$ at 4.2 K; we then fit σ_1/σ_n with Δ as the sole fitting parameter. For some of the samples, the behavior of $\sigma_1(\omega)$ at subgap frequencies $\omega < 2\Delta/\hbar$ slightly deviates from MB and therefore is excluded from the fit. We then fit $\Delta(T)$ to the standard BCS gap equation [20] with $\Delta(0)$ as the sole fitting parameter, without any restriction on the coupling ratio $2\Delta(0)/k_B T_c$. The

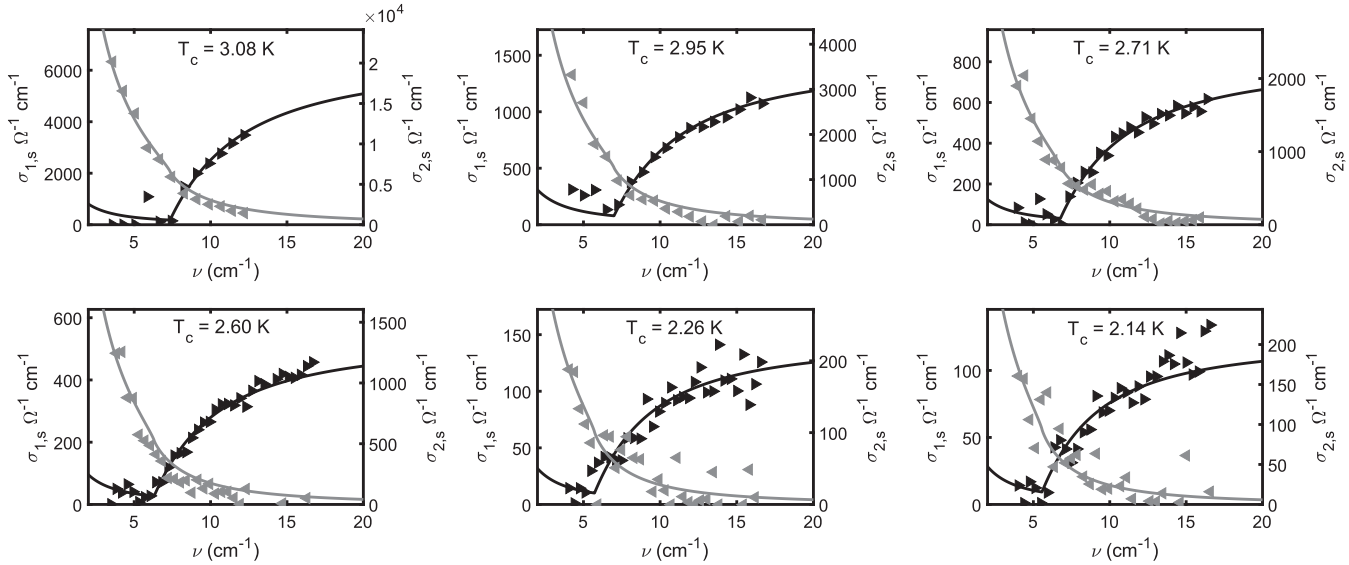

FIG. 5. Optical conductivity $\hat{\sigma}(\omega)$ of all samples. The black triangles and line are the real part of the conductivity and its MB fit; the gray triangles and line are the imaginary part of the conductivity and its MB fit. The data are shown for $T = 1.5$ K, except for sample 2 ($T_c = 2.95$ K), which was measured down to $T = 1.7$ K.

complex conductivity for all samples at the lowest measured temperature along with its MB fit is shown in Fig. 5, with good agreement for all samples.

IV. DISCUSSION

First of all, we compare our results to tunneling data. The value of the optical gap as determined from fitting the conductivity data to the MB theory is close to the value of the tunneling gap reported by Abeles and Hanak [21]. According to them, the coupling ratio $2\Delta(0)/k_BT_c$ is equal to 3.4 for all specimens within 2%. In fact, according to the optical gap values reported in Table I, the coupling ratio increases continuously with resistivity, a trend already noted by Pracht *et al.* [9] for a high-resistivity sample. This deviation appears to be systematic, with the coupling ratio varying from 3.56 for the lowest-resistivity sample (close to the weak-coupling value of 3.53) up to 4.51 for the highest-resistivity one. This is one of our main findings.

Second of all, we compare our results with those obtained by Cheng *et al.* on disordered NbN films [3]. As can be seen in Fig. 7, as the resistivity [and $(k_Fl)^{-1}$] increases, the coupling ratio *decreases* continuously, rather than increasing. Furthermore, the value of the optical gap becomes distinct from and smaller than the tunneling gap. At the highest resistivity investigated ($\sim$1000 $\mu\Omega$ cm), there is not even a clear optical gap edge. This difference in behavior between the optical data obtained on granular Al and NbN is emphasized in Fig. 8, where $\hbar\omega$ has been scaled by twice the value of the tunneling gap. While for granular Al the conductivities scale fairly, they clearly do not for NbN.

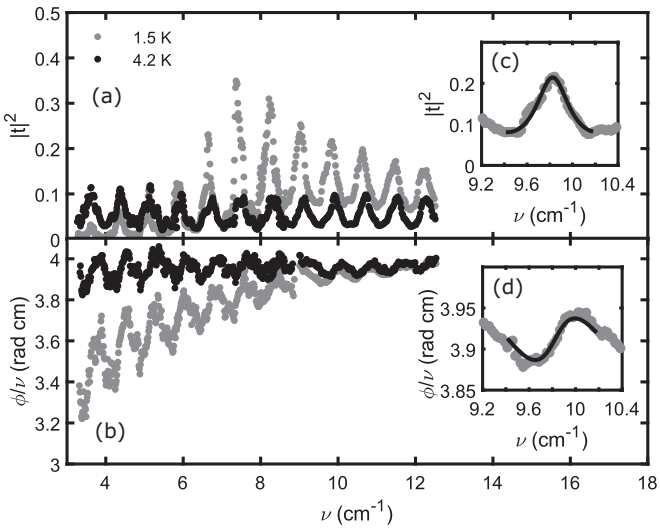

FIG. 6. Raw data of sample 1. (a) Transmittance; (b) phase divided by frequency in the normal (black) and SC (gray) states. Insets (c) and (d) show an example of the resulting simultaneous fit to both $|t|^2$ and ϕ_t/ν (black line) by σ_1, σ_2 of the film.

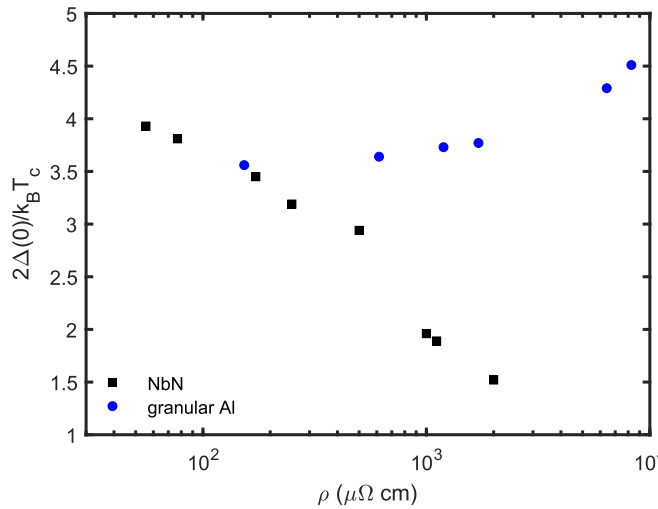

FIG. 7. Coupling ratio vs resistivity. Black squares are NbN data from Ref. [3] and blue circles are our granular Al data.

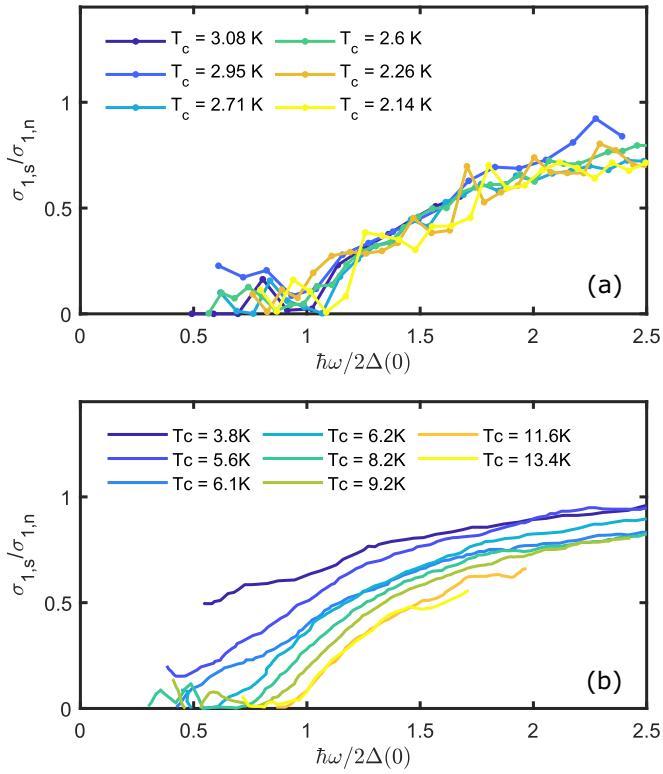

FIG. 8. Real part of the optical conductivity, measured at the lowest temperature, normalized to the normal-state conductivity. The frequency axis is normalized to twice the value of the tunneling gap. (a) Our granular Al data; (b) Cheng *et al.* NbN data [3].

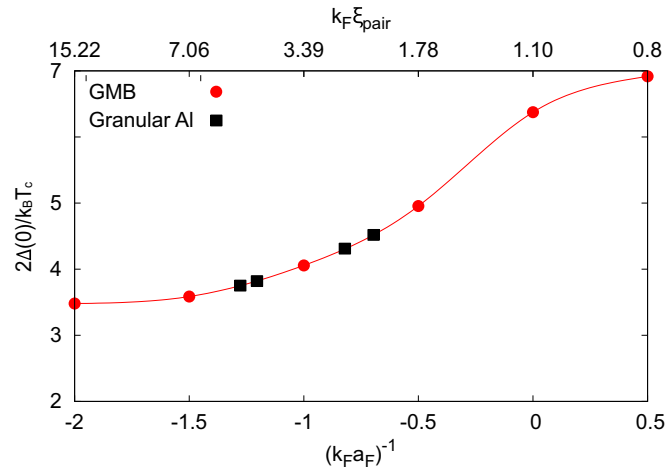

FIG. 9. The coupling ratio as a function of $k_F\xi_{\rm pair}$ or $(k_Fa_F)^{-1}$ (Pisani *et al.* [26]). The red circles (●) are the results of the numerical calculations that include corrections beyond mean field which arise from pairing fluctuations, labeled GMB. The red line joining these circles is a guide to the eye. The black squares (■) correspond to our measured coupling ratio. The corresponding values of $(k_Fa_F)^{-1}$ range from -1.3 to -0.7 and those of $k_F\xi_{\rm pair}$ from 5.3 to 2.3.

These points deserve a detailed discussion.

Regarding the first one, the increase of the coupling ratio seen in granular Al with resistivity may have two different origins. The first one would be a stronger coupling to soft phonons often cited as the possible reason for the higher T_c of granular films [22]. However, we discard this interpretation here since the critical temperature is decreasing in our series of high-resistivity samples. A second origin would be an approach to a BCS-to-BEC crossover. In the case of a BE condensation, the pair-breaking energy becomes disconnected from the k_BT_c energy scale, which is much smaller. In the crossover regime from BCS to BE condensation, the coupling ratio becomes progressively larger than the weak-coupling limit value. This effect has been studied recently in detail by Pisani *et al.* [1,2] who have calculated how T_c/E_F, the zero-temperature gap $\Delta(0)/E_F$, and $\frac{2\Delta}{k_BT_c}$ vary with the distance to the unitary limit, where the product of the Fermi wave vector k_F by the scattering length a_F goes to infinity. We note that it is possible to describe the crossover in terms of the variable $k_F\xi_{\rm pair}$ [23], which has been calculated as a function of $(k_Fa_F)^{-1}$ [24].

We favor this second interpretation. The idea is that in the granular case, confinement results in strong coupling in the sense that the coherence length can become so short that there are only a few pairs in a coherence volume, which is what happens at a BCS-to-BEC crossover. When the coupling ratio reaches the value of 4.51, as is the case for our highest-resistivity sample, $(k_Fa_F)^{-1} \simeq -0.70$, or $k_F\xi_{\rm pair} \simeq 2.28$ according to Pistolesi *et al.* [23], not far from the unitary limit. Figure 9 shows the coupling ratios of samples 3–6; for samples 1 and 2, the coupling ratio is insensitive to variation in $(k_Fa_F)^{-1}$ and therefore is not shown. We use the measured coupling ratio to evaluate E_F and therefore k_F (assuming that the effective mass is not too different from that of a bare electron). For our most resistive sample, $\Delta(0)/E_F = 0.17$, which yields $E_F = 2.47$ meV and $k_F = 2.54 \times 10^8$ m^{-1}. Upper critical field measurements of similar samples [25] yield a coherence length of about $\xi_0 \simeq 10$ nm $\simeq \xi_{\rm pair}$. We obtain $k_F\xi_{\rm pair} = 2.54$, which is close to the value obtained by the coupling ratio alone. A reduced effective Fermi energy was previously inferred from the negative magnetoresistance seen in granular Al films. It was analyzed in terms of the presence of diluted magnetic impurities [8], but this model does not apply when k_Fl is smaller than unity, as is the case here. This may be the reason why the reduction in E_F was not as strong as seen here.

Concerning the second point, one can understand the difference in behavior between granular Al and disordered NbN films as resulting from their different disorder length scales, being respectively the grain size in granular Al and the lattice parameter or interatomic distance in NbN. In a three-dimensional (3D) system, the metal-to-insulator transition occurs when the conductivity g measured at the relevant length scale crosses a critical value g_c. Here, g is the universal conductance $\frac{2e^2}{h}$ divided by the relevant length scale d. Since the grain size in granular Al is about one order of magnitude larger than the interatomic distance in NbN, it follows that the value of the critical conductivity in the former is expected to be about one order of magnitude smaller than in the latter. However, this argument does not explain the qualitative difference between the behaviors of the optical conductivities of granular Al and NbN seen in Fig. 8. As the M-I transition is approached, a sharp gap edge persists in granular Al, but not in

NbN. This suggests that the nature of the M-I transition is not the same in the two systems. While it is of the Anderson type in NbN, we believe that it is of the Mott type in granular Al, as already proposed [8]. This is consistent with the large value of the coupling ratio, since at a Mott transition the effective bandwidth reduces to zero (while the density of states (DOS) at the Fermi level remains finite [27]). As the bandwidth reduces, the coupling ratio increases for any finite value of the gap. In dynamical mean-field theory (DMFT) models, the ratio of the Coulomb energy to the bandwidth is close to 3 when the transition occurs [27]. In the granular case, the value of the Coulomb energy is that of the electrostatic energy of the grains, which for a 2-nm-size grain is about 30 meV [28]. An effective bandwidth of 10 meV is compatible with the value of 2.5 meV for the Fermi energy deduced from the value of the strong-coupling ratio. We note that the energy-level splitting is also about 10 meV.

We may add that the coherence length in NbN is always much larger than the disorder length scale, so that the system never approaches the BCS-to-BEC crossover and therefore never develops the strong-coupling effect predicted by Pisani *et al.* [1,2]. In fact, in NbN, the coherence length increases when the metal-to-insulator transition is approached [29]. It is worthwhile to note that Cao *et al.* [30] showed that in a superlattice made from "magic-angle" twisted bilayer graphene (TBG), superconductivity appears as the TBG is doped slightly away from the Mott-like insulator state. In the superconducting state, a proximity to BCS-BEC crossover is possible, supported by $\xi \approx 50$ nm and interparticle spacing of about 26 nm.

V. CONCLUSION

Optical spectroscopy reveals that a sharp gap edge persists in granular aluminum films as the metallic grains are being decoupled towards the metal-to-insulator transition. Remarkably, at the same time, the coupling ratio $2\Delta(0)/k_BT_c$ increases, reaching in the most resistive sample a value consistent with an approach to the unitary limit. The critical temperature is not strongly reduced by the grain decoupling. This behavior is consistent with a Mott transition driven by the electrostatic charging energy of the grains.

This behavior is in contrast with that observed previously in atomically disordered NbN film, where the coupling ratio reduces when disorder is increased, the critical temperature goes down strongly, and the sharp gap edge vanishes, a behavior consistent with an Anderson transition [7]. The origin of the good performance of high kinetic inductance granular Al resonators reported recently [6] may be due to the fact that the M-I transition is of the Mott type rather than of the Anderson type. This granular system may indeed be viewed as a network of Josephson junctions between well-defined Al grains, as suggested by Grünhaupt *et al.* [6], rather than as a highly disordered superconductor.

ACKNOWLEDGMENTS

We acknowledge G. C. Strinati for fruitful discussion and for supplying us with the Fig. 9 data. We are grateful to N. Bachar for guidance with early sample preparation and THz measurements.

[1] L. Pisani, P. Pieri, and G. C. Strinati, Phys. Rev. B **98**, 104507 (2018).
[2] L. Pisani, A. Perali, P. Pieri, and G. C. Strinati, Phys. Rev. B **97**, 014528 (2018).
[3] B. Cheng, L. Wu, N. J. Laurita, H. Singh, M. Chand, P. Raychaudhuri, and N. P. Armitage, Phys. Rev. B **93**, 180511(R) (2016).
[4] D. Sherman, U. S. Pracht, B. Gorshunov, S. Poran, J. Jesudasan, M. Chand, P. Raychaudhuri, M. Swanson, N. Trivedi, A. Auerbach, M. Scheffler, A. Frydman, and M. Dressel, Nat. Phys. **11**, 188 (2015).
[5] D. C. Mattis and J. Bardeen, Phys. Rev. **111**, 412 (1958).
[6] L. Grünhaupt, N. Maleeva, S. T. Skacel, M. Calvo, F. Levy-Bertrand, A. V. Ustinov, H. Rotzinger, A. Monfardini, G. Catelani, and I. M. Pop, Phys. Rev. Lett. **121**, 117001 (2018).
[7] M. Mondal, A. Kamlapure, M. Chand, G. Saraswat, S. Kumar, J. Jesudasan, L. Benfatto, V. Tripathi, and P. Raychaudhuri, Phys. Rev. Lett. **106**, 047001 (2011).
[8] N. Bachar, S. Lerer, A. Levy, S. Hacohen-Gourgy, B. Almog, H. Saadaoui, Z. Salman, E. Morenzoni, and G. Deutscher, Phys. Rev. B **91**, 041123(R) (2015).
[9] U. S. Pracht, N. Bachar, L. Benfatto, G. Deutscher, E. Farber, M. Dressel, and M. Scheffler, Phys. Rev. B **93**, 100503(R) (2016).
[10] N. Bachar, U. Pracht, E. Farber, M. Dressel, G. Deutscher, and M. Scheffler, J. Low Temp. Phys. **179**, 83 (2015).
[11] U. S. Pracht, E. Heintze, C. Clauss, D. Hafner, R. Bek, D. Werner, S. Gelhorn, M. Scheffler, M. Dressel, D. Sherman, B. Gorshunov, K. S. Il'in, D. Henrich, and M. Siegel, IEEE Trans. Terahertz Sci. Technol. **3**, 269 (2013).
[12] M. Dressel and G. Gruner (eds.), *Electrodynamics of Solids* (Cambridge University Press, Cambridge, 2002).
[13] N. Bachar, S. Lerer, S. Hacohen-Gourgy, B. Almog, and G. Deutscher, Phys. Rev. B **87**, 214512 (2013).
[14] G. Deutscher, M. Gershenson, E. Grünbaum, and Y. Imry, J. Vac. Sci. Technol. **10**, 697 (1973).
[15] G. Deutscher, H. Fenichel, M. Gershenson, E. Grünbaum, and Z. Ovadyahu, J. Low Temp. Phys. **10**, 231 (1973).
[16] D. Gall, J. Appl. Phys. **119**, 085101 (2016).
[17] B. Gorshunov, A. Volkov, I. Spektor, A. Prokhorov, A. Mukhin, M. Dressel, S. Uchida, and A. Loidl, Int. J. Infrared Mill. Waves **26**, 1217 (2005).
[18] S. Arezoomandan, A. Prakash, A. Chanana, J. Yue, J. Mao, S. Blair, A. Nahata, B. Jalan, and B. Sensale-Rodriguez, Sci. Rep. **8**, 3577 (2018).
[19] U. S. Pracht, T. Cea, N. Bachar, G. Deutscher, E. Farber, M. Dressel, M. Scheffler, C. Castellani, A. M. Garcia-Garcia, and L. Benfatto, Phys. Rev. B **96**, 094514 (2017).
[20] J. Bardeen, L. N. Cooper, and J. R. Schrieffer, Phys. Rev. **108**, 1175 (1957).
[21] B. Abeles and J. Hanak, Phys. Lett. A **34**, 165 (1971).

[22] J. W. Garland, K. H. Bennemann, and F. M. Mueller, Phys. Rev. Lett. **21**, 1315 (1968).
[23] F. Pistolesi and G. C. Strinati, Phys. Rev. B **49**, 6356 (1994).
[24] G. C. Strinati, P. Pieri, G. Ropke, P. Schuck, and M. Urban, Phys. Rep. **738**, 1 (2018).
[25] S. Lerer, N. Bachar, G. Deutscher, and Y. Dagan, Phys. Rev. B **90**, 214521 (2014).
[26] L. Pisani, A. Perali, P. Pieri, and G. C. Strinati (private communication, 2018).
[27] A. Georges, G. Kotliar, W. Krauth, and M. J. Rozenberg, Rev. Mod. Phys. **68**, 13 (1996).
[28] B. Abeles, Phys. Rev. B **15**, 2828 (1977).
[29] M. Chand, G. Saraswat, A. Kamlapure, M. Mondal, S. Kumar, J. Jesudasan, V. Bagwe, L. Benfatto, V. Tripathi, and P. Raychaudhuri, Phys. Rev. B **85**, 014508 (2012).
[30] Y. Cao, V. Fatemi, S. Fang, K. Watanabe, T. Taniguchi, E. Kaxiras, and P. Jarillo-Herrero, Nature (London) **556**, 43 (2018).